Waveguide integrated GaN distributed Bragg reflector cavity using low-cost nanolithography

Simeng Jia[1] ✉, *Emmanuel D. Le Boulbar*[2], *Krishna C. Balram*[1], *Jon R. Pugh*[1], *Tao Wang*[3], *Duncan W.E. Allsopp*[2], *Philip A. Shields*[2], *Martin J. Cryan*[1]

[1]*Department of Electrical and Electronic Engineering, University of Bristol, Bristol BS8 1UB, UK*
[2]*Department of Electrical and Electronic Engineering, University of Bath, Bath BA2 7AY, UK*
[3]*Department of Electronic and Electrical Engineering, University of Sheffield, Sheffield S1 4DE, UK*
✉ *E-mail: simeng.jia@bristol.ac.uk*

Published in Micro & Nano Letters; Received on 14th June 2019; Revised on 6th August 2019; Accepted on 6th September 2019

This work presents the design, fabrication and measurement of gallium nitride (GaN) distributed Bragg reflector cavities integrated with input and output grating couplers. The devices are fabricated using a new, low-cost nanolithography technique: displacement Talbot lithography combined with direct laser writing lithography. The finite-difference time-domain method has been used to design all the components and measured and modelled results show good agreement. Such devices have applications in GaN integrated photonics and biosensing.

1. Introduction: Gallium nitride (GaN) is a promising candidate for many integrated photonics applications [1–6]. It is transparent from ~400 nm to ~13.6 μm [7], has a relatively high refractive index of ~2.4 and is used as the basis for a range of visible LEDs and lasers [8–12], including vertical cavity surface emitting lasers [13]. These unique properties have been used in photonic integrated circuits and led to recent work developing GaN as a chemical and biological sensing platform [14]. GaN-based waveguides have achieved low loss [15, 16] and have been implemented as freestanding waveguide structures [17–19]. GaN-based photonic crystal cavities have also been developed and high Q factors have been obtained which can be used to sense biological or chemical analytes [20, 21]. Although the technology of GaN waveguides is not as mature as silicon-on-insulator [22], the characteristics of GaN discussed above act as an impetus to further explore photonic integrated circuits in this technology. The fabrication of GaN waveguides and photonic crystal cavities is almost always based on electron beam lithography. Although the accuracy of this method is very high, the manufacturing process is slow and is very expensive. This work aims to design a waveguide integrated GaN distributed Bragg reflector (DBR) cavity using a new nanolithography technique: displacement Talbot lithography (DTL), which can produce large area, nanoscale periodic structures with low-cost and high-throughput [23, 24]. Basic results were shown in [25], here we show in-depth modelled and measured results along with fabrication details and waveguide loss measurements.

The proposed structure is shown in Fig. 1, which includes two GaN gratings couplers and two GaN DBR gratings forming a cavity. The use of DTL fabrication restricts the period of all gratings to be nominally the same across the whole wafer, with laser lithography being used to define the region where the gratings are present. In future structures it may be possible to have different etch depths for different gratings, but here we have restricted processing a single etch step. These limitations are not ideal for forming both grating couplers and DBR cavities, but compared to the very high cost of electron-beam lithography, DTL + DLW (direct laser writing) is an interesting much lower cost option and this Letter shows the potential for this approach.

2. Grating couplers

2.1. Modelling and design: We used the two-dimensional finite-difference time-domain (FDTD) technique from Lumerical FDTD Solutions [26] to optimise the maximum out coupled power for a 1.5 μm layer of GaN-on-Sapphire. Fig. 2 shows the 2D schematic cross-section for the in–out grating coupler structure.

In the model, a fundamental transverse electric (TE_0) mode source comes from a fibre which is single mode around the wavelength of interest which is 630–640 nm. This was initially based on the fact that a red laser would be used to show simple light coupling, this was eventually replaced with a supercontinuum laser source. Thus, the fibre is a SMF600 with 125 μm cladding diameter and 4.3 μm core diameter. Light from the fibre will be diffracted into the reflected and transmitted orders. Some of the transmitted orders which satisfy the guided mode conditions can propagate in the 120 μm long waveguide and be coupled out into free space, then collected by an identical single-mode fibre at the output. The simulation uses a wavelength range of 450–900 nm and is mainly focused on optimising across the 630–640 nm wavelength range. The gratings and waveguide are in the GaN layer with a refractive index $n_{GaN} = 2.38$ [27]. The substrate is sapphire with a refractive index $n_{Sapphire} = 1.77$ [28], and the cover region is air.

There are four main design parameters for the grating couplers: grating period, filling factor, etch depth and number of periods, where grating period $\Lambda = L_1 + L_2$ and filling factor $a = L_1/\Lambda$. In addition, the fibre angle of incidence plays an important role. In our case this was fixed at 15° based on the available optical measurement set up. The main design choice to be made is the grating period and diffraction theory can be used to determine the optimum value and this is simplest when the waveguide is single mode [29]. However, in our case the GaN slab waveguide is highly multimode, supporting 8 TE modes around 630–640 nm wavelength. Thus in our case, we based our choice on available DTL masks and decided on a 400 nm period grating. FDTD modelling was then used to determine the impact of etch depth and filling factor in order to guide the fabrication process. The number of periods was chosen as 45 giving a grating length of 18 μm which was felt to be sufficiently large with respect to the fibre core diameter of 4.3 μm. A waveguide length of 120 μm was chosen as a balance between simulation memory requirements and obtaining realistic results for waveguides that would be much longer in practice. In the FDTD modelling, by varying the etch depth ranging from 0 to 1500 nm and fill factor from 0.2 to 0.8, it was found that the TE_0 mode input source has an optimum in–out transmittance at 640 nm wavelength when the fill factor is

doi: 10.1049/mnl.2019.0366

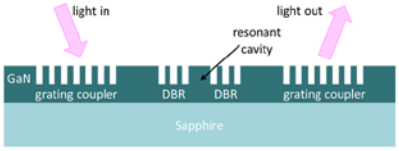

Fig. 1 *Schematic representation of the proposed grating coupled DBR cavity*

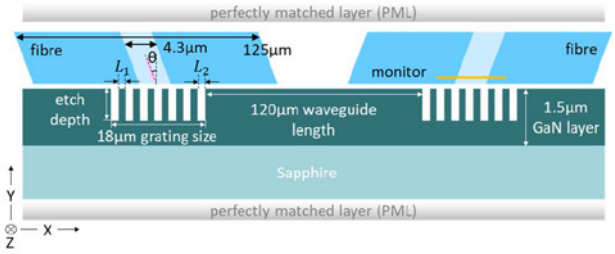

Fig. 2 *Geometry of 1.5 μm GaN on sapphire in–out grating couplers. Device parameters:* $n_{GaN} = 2.38$, $n_{sapphire} = 1.77$, *grating period=* $L_1 + L_2 = 400$ *nm, filling factor=*$L_1/(L_1 + L_2)$, *grating length = 18 μm, number of periods = 45, waveguide length = 120 μm*

0.45 and the etch depth is 600 nm. Fig. 3 shows the transmittance spectra for the TE_0 mode, fundamental transverse magnetic (TM_0) mode and $TE_0 + TM_0$ modes sources with these parameters. It can be seen that the TE_0 mode has high transmission and the TM_0 mode has very low transmission. This would allow us to use unpolarised light at the input and restrict the waveguide and cavity design to TE modes only. In the TE_0 case, a number of peaks in transmittance are obtained in four wavelength regions: 480–530, 610–660, 660–720 and 720–780 nm. Here, the best transmittance is 0.109 or −9.65 dB at 634.5 nm wavelength. The bandwidth for this peak is about 10.5 nm. The transmittance of TM_0 mode is almost zero, especially near the wavelength of 640 nm. In order to model the transmission of unpolarised light we can sum the TE and TM results as shown in Fig. 3.

2.2. Fabrication: Since the process was to employ only a single GaN etch step using a 450 nm-thick plasma-enhanced chemical vapour deposition SiN_x hard etch mask, multiple lithography

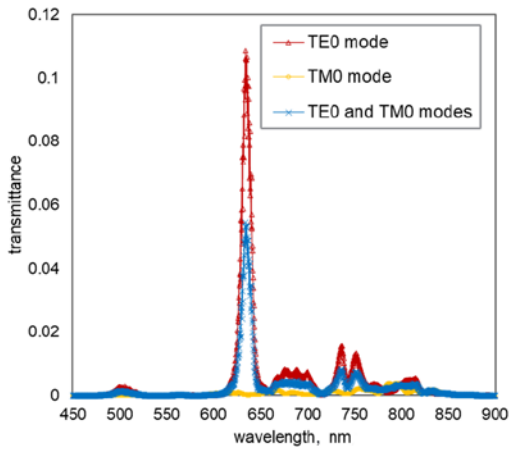

Fig. 3 *2D FDTD modelling transmittance result for in–out coupling at 15° angle of incidence. Geometry of 1.5 μm GaN on sapphire in–out grating couplers. Device parameters:* $n_{GaN} = 2.38$, $n_{sapphire} = 1.77$, *waveguide length = 120 μm, grating length = 18 μm, grating period = 400 nm, filling factor = 0.45, etch depth = 600 nm*

steps were required to pattern the SiN_x mask beforehand. This is due to the different capabilities of the two lithography techniques: DTL can pattern periodic nanoscale features but only with large areas, whereas DLW can pattern arbitrary features >∼1 μm. Three different regions on the mask are required: large areas of SiN_x to protect the waveguide, grating patterns for the couplers and the DBRs, and large unprotected areas in order to surround the waveguide.

The first step of the fabrication process was to define the large waveguide features in the mask. A S1813 positive photoresist mask was patterned via DLW (μPG 101, Heidelberg Instruments) and then transferred into the SiN_x via ICP etching using CHF_3 chemistry. This resist was then removed before applying a second, 350 nm-thick, high-resolution, AZ15NXT negative photoresist layer (on top of a Wide 8C bottom anti-reflective coating to improve resolution). This was exposed via DTL (PhableR 100C, EULITHA) to create a 400 nm-pitch grating in the resist across the whole sample area. A second exposure via DLW then fully exposed the negative resist in all areas where gratings were not required before CHF_3 plasma was used to transfer the resist pattern into the SiN_x. In this way, small grating regions could be created in the SiN_x whilst the negative resist protected the surrounding sample. The resist was subsequently removed.

The resulting SiN_x was used as a mask to etch ∼780 nm of GaN using Cl_2/Ar plasma. A high etch temperature of 150°C was used to ensure vertical sidewall etch profiles [30]. Finally, the SiN_x mask was stripped in HF-based solution.

Fig. 4 shows scanning electron microscopy (SEM) pictures of typical grating couplers. The filling factor is shown for one grating coupler and is seen to be close to 0.5. The etch depth has been estimated to be 780 nm. Fig. 5 shows the input coupling transmittance maps at a wavelength of 640 nm. It shows the dependence of TE_0 and TM_0 modes on etching depth and filling factor, respectively. Here, the position of the red box is the best optimisation parameters mentioned in Fig. 3, and the position of the white box is the parameters obtained with the DTL fabrication. Fig. 6 shows the simulated in–out transmittance for TE_0 mode, TM_0 mode and $TE_0 + TM_0$ modes sources with these parameters. The figure shows that both TE_0 mode and TM_0 mode have good transmittance around 630–640 nm wavelength with these structural parameters. This will complicate the operation of the device; in future work we will use polarisation controllers to restrict measurement to a single polarisation, but here we will continue to use unpolarised light.

2.3. Measurement: Optical testing was performed using the measurement setup shown in Fig. 7. The chip is placed on a XYZ translation stage. Two single mode optical fibres (SMF600) are mounted at an angle of 15° which couple light into and out of the chip. A SuperK COMPACT supercontinuum laser delivers

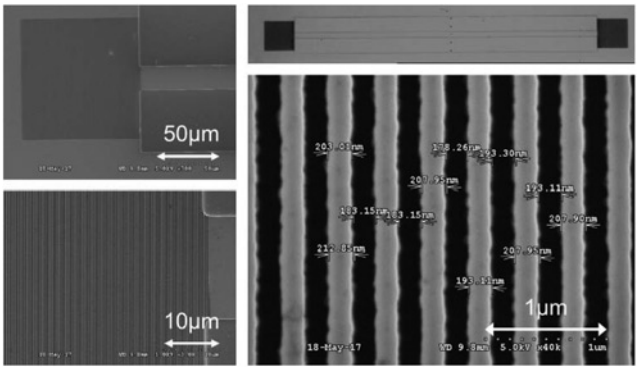

Fig. 4 *SEM images of typical grating couplers and waveguides after DTL and DLW processing*

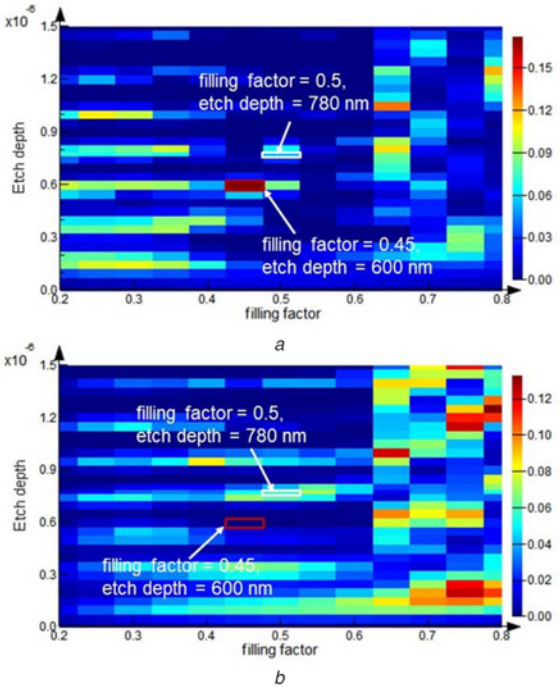

Fig. 5 *2D FDTD modelling transmittance map for input coupling at 15° angle of incidence with varying the filling factor (x-axis) and etch depth (y-axis). Device parameters: $n_{GaN} = 2.38$, $n_{sapphire} = 1.77$, grating length = 18 µm, grating period = 400 nm*
a TE_0 at a wavelength of 640 nm
b TM_0 at a wavelength of 640 nm

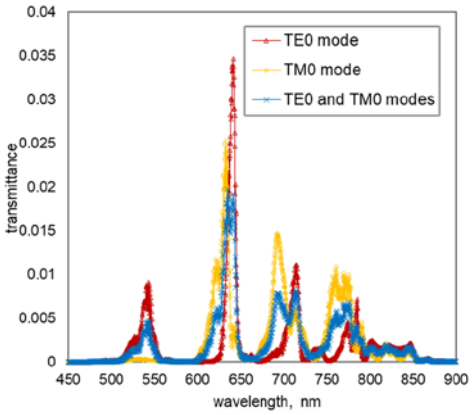

Fig. 6 *2D FDTD modelling transmittance result for in–out coupling at 15° angle of incidence. Device parameters: $n_{GaN} = 2.38$, $n_{sapphire} = 1.77$, waveguide length = 120 µm, grating length = 18 µm, grating period = 400 nm, filling factor = 0.5, etch depth = 780 nm*

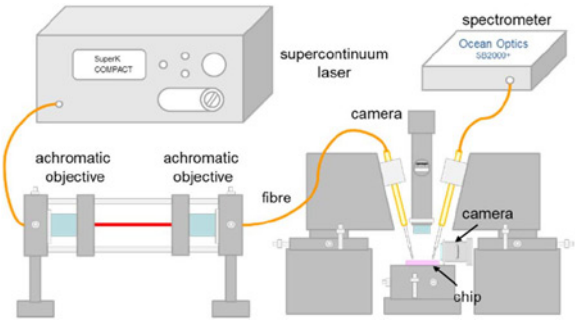

Fig. 7 *Fibre-based measurement set up which includes a supercontinuum laser, two achromatic objectives, two single mode fibres, chip, detector and two cameras*

the unpolarised light to the input fibre. To avoid the possibility that direct coupling damages the fibre facet, two achromatic objectives are added to couple from laser into free-space, then into the fibre. An Ocean Optics spectrometer is used to collect in–out coupling intensity data. A high-magnification camera is used to show a plan-view and the location of fibres on the sample. The second camera shows a side-view to check the vertical distance between the fibre facets and sample.

The layout of part of the chip is shown in Fig. 8. A series of 100 µm × 100 µm area grating couplers with varying waveguide lengths are located in this area.

The plan-view image of GaN grating couplers and waveguide is shown in Fig. 9*a*. The output grating can be seen to be bright in Fig. 9*b* when the output fibre is removed, showing that reasonable coupling has been obtained.

The in–out coupling measurement results with varying waveguide length are shown in Fig. 10*a*. It can be seen that there are two regions of high transmittance around 640 and 700 nm and this matches up well with the $TE_0 + TM_0$ mode result shown in Fig. 6. There is some variation in the peak wavelength between the 6 waveguide lengths, but this is expected due to the fabrication differences between gratings in the different waveguides. In the case of the 1 mm waveguide there is a strong ripple with a peak spacing of 4.1 nm. It is believed that this ripple is related to mode beating [31] between the multiple modes that can propagate in the waveguide and the mode spacing is of the order that would be expected for this length of waveguide. The longer waveguides do not have such a prominent ripple, but these will have higher loss, and this will tend to suppress the mode beating effect.

The coupling loss and waveguide attenuation are estimated by the cutback method. In order to accurately calculate the coupling loss, the input fibre should be connected directly to the output to act as a reference, however in our current set up this was not possible. Thus, in order to make an approximate estimate for coupling loss, a silver mirror placed in the position of the chip was used as a reference. This will significantly underestimate the coupling loss and in future work we will improve this coupling loss estimate. Fig. 10*b* shows the transmittance at 639 nm normalised to the mirror transmittance for each waveguide length. In the case of the 1 mm length, due to the strong ripple an estimate was

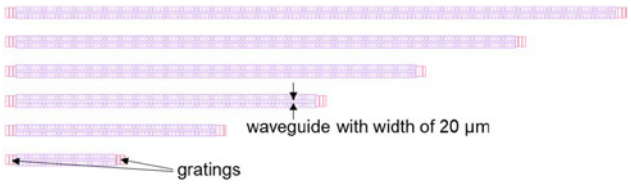

Fig. 8 *Layout of part of the chip: grating couplers with straight waveguides. Device parameters:100 µm × 100 µm grating couplers, grating period = 400 nm, waveguide width = 20 µm, waveguide length from 1 to 6 mm (in steps of 1 mm)*

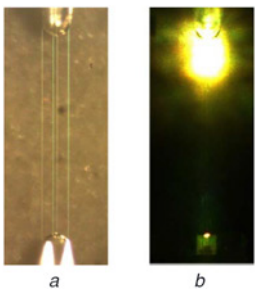

Fig. 9 *Image of grating couplers with 1 mm waveguide plan-view*
a In–out coupling setup plan-view
b Output grating is bright when the output fibre is removed

doi: 10.1049/mnl.2019.0366

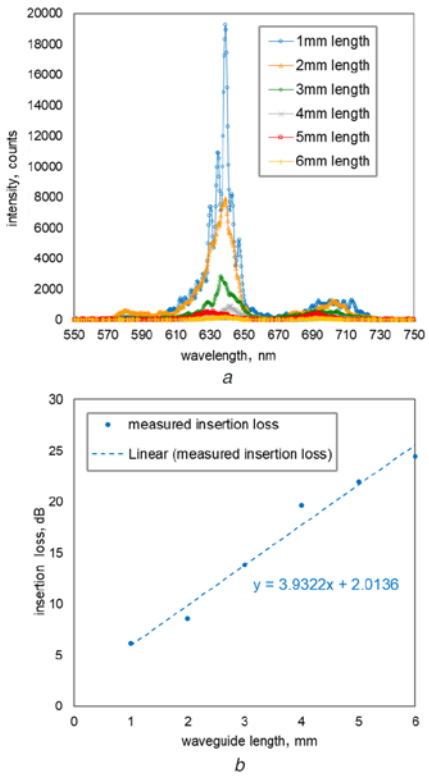

Fig. 10 *Measured in–out coupling results*
a Measured output intensity for 20 µm width waveguide in–out coupling with varying waveguide lengths
b Coupling loss and waveguide attenuation estimation using the cut-back method

required which removed the effect of these ripples. The slope of the linear fit gives the waveguide loss to be 3.9 dB/mm. The coupling loss, compared to the mirror transmittance, is obtained as the intercept with the vertical axis and is found to be 2 dB in total or 1 dB per coupler.

3. DBR cavity

3.1. Modelling and design: Next, we focus on the DBR cavity design. The schematic representation of an isolated cavity is shown in Fig. 11. It consists of two 400 nm period DBR gratings forming a cavity. As described above, we represent unpolarised light with a $TE_0 + TM_0$ mode source. The length of the cavity was chosen to be 8 µm, ensuring that there is sufficient length to observe resonant peaks, and the filling factor and etch depth remain unchanged at 0.5 and 780 nm, respectively.

The modal transmittance of Fig. 12 is for 25 period DBR gratings with an 8 µm cavity. A mode spacing of ~10 nm can be seen at an etch depth of 780 nm around 640 nm wavelength which will allow approximately two resonant peaks to be observed in the bandwidth

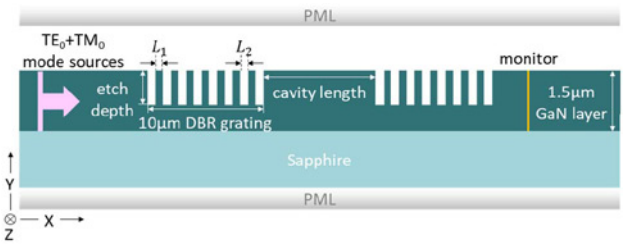

Fig. 11 *Geometry of two DBR gratings with 8 µm cavity. Device parameters: grating period* $= L_1 + L_2 = 400$ *nm, filling factor*$= L_1/(L_1 + L_2) = 0.5$, *DBR grating size = 10 µm*

of the grating coupler, shown in Fig. 10*a*. It can be seen that 780 nm etch depth is an optimum for resonant cavity behaviour. In order to understand these effects further, we can use FDTD to look at the fields at one of the resonant peaks, shown in Fig. 13.

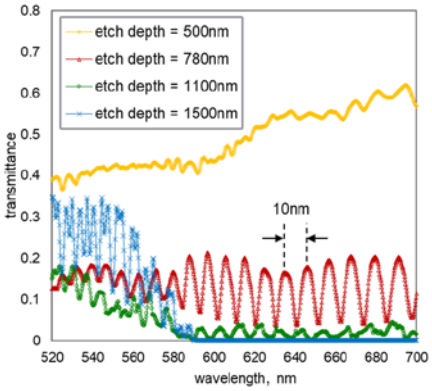

Fig. 12 *Simulated* $TE_0 + TM_0$ *mode sources transmittance spectra of DBRs cavity with varying etch depth, filling factor = 0.5, cavity length = 8 µm*

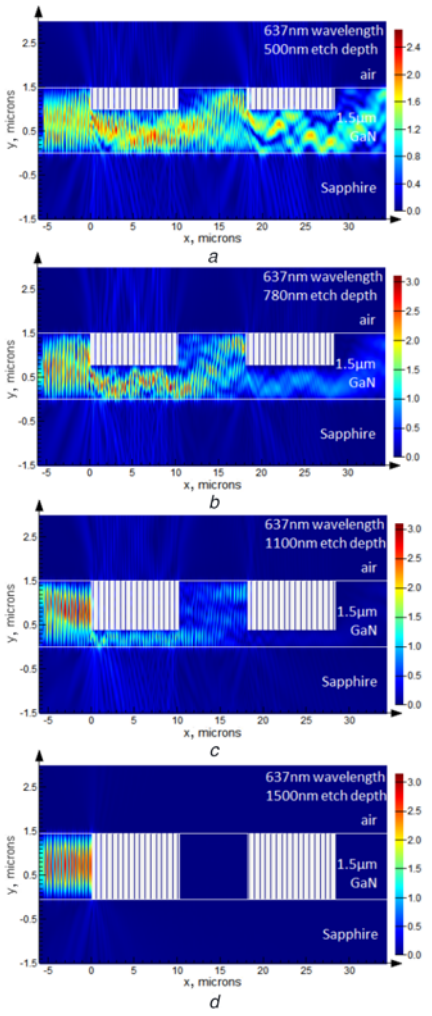

Fig. 13 E_z *field distribution in cross-section for the peak wavelength (637 nm),* $TE_0 + TM_0$ *modes propagating from left to right. Grating parameters: filling factor = 0.5, period = 400 nm, cavity length = 8 µm (vertical and horizontal axes not to scale)*
a Etch depth = 500 nm
b Etch depth = 780 nm
c Etch depth = 1100 nm
d Etch depth = 1500 nm

Fig. 13 shows the magnitudes of the E_z field for $TE_0 + TM_0$ modes with different etch depths at wavelength of 637 nm which is one of the resonance peaks. At 500 nm etch depth, because the structure is not fully etched, most of the light propagates in the region beneath the Bragg grating and does not couple into the cavity, so as shown in Fig. 12, no obvious resonance peaks are observed. As the etching becomes deeper, more light couples into the cavity and at a depth of 780 nm a significant amount of light is coupled into the cavity and this results in the resonances observed in Fig. 12. As the etch becomes deeper, the amount of light propagating through the first DBR decreases significantly and this reduces the resonant behaviour and in the case of full etching, removes any resonances completely. It can be seen that since the waveguide is multimode, very non-ideal operation is observed for this structure. In future work, thinner GaN layers and ridge waveguide structures will be used to ensure single mode operation which will simplify device operation significantly.

Fig. 14 shows the layout for one DBR cavity on the chip and Fig. 15 shows an SEM picture of a typical 10 µm long cavity. There are some unetched portions of the DBRs which will cause some differences between measured and modelled results.

3.2. Measurement: The zoomed in–out coupling with DBR cavity measurement results is shown in Fig. 16 for two different devices on the same chip and it can be seen that similar performance is obtained. However, a mode spacing of 10 nm is observed in one case, but not for the second device. Since the waveguide is highly multimode, the mode spacing will depend on which modes are resonating in the cavity and the defects shown in Fig. 15 will also produce non-ideal results. Insets show visible light camera images of both cavities which shows significant scattering from the first DBR and evidence of the high-intensity peaks within the cavity.

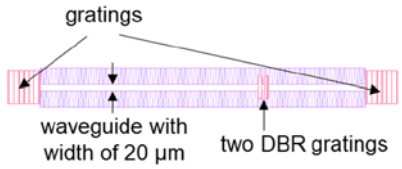

Fig. 14 *Layout of part of the chip: grating couplers with DBR cavity. Device parameters: 100 µm × 100 µm coupling grating size, DBR grating length = 10 µm, DBR grating width = 60 µm, grating period = 400 nm, cavity length = 8 µm, waveguide width = 20 µm, waveguide length = 1 mm*

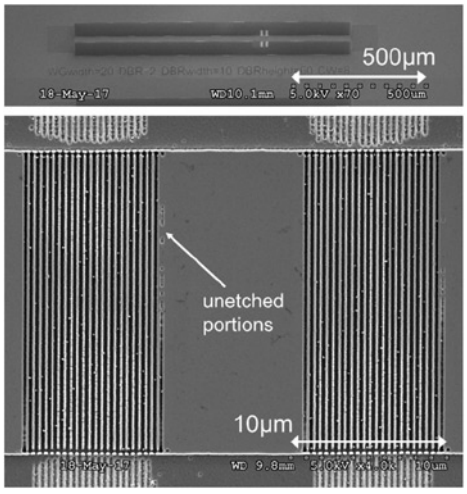

Fig. 15 *SEM image of a DBR resonant cavity*

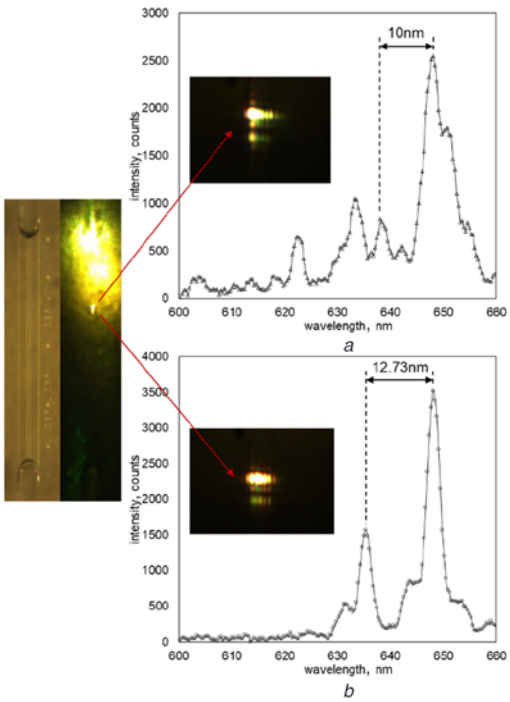

Fig. 16 *Zoom-in of measured in–out coupling for two different cavities and visible light images of light scattered from the cavities*
a Device 1
b Device 2

4. Conclusion: This Letter has shown GaN DBR cavities with grating couplers fabricated using DTL. Cavities with Q factors of >200 have been measured which show the potential for this route to low-cost commercial sensor applications. In future work, single-mode waveguides will be fabricated which will result in much more idealised grating coupler and cavity behaviour which will lead to increased device performance. The main restriction for the DTL approach is that all gratings must have the same period, but with correct processing, different etch depths and fill factors could be obtained which would further improve the device performance.

5. Acknowledgments: This work was supported by Engineering and Physical Sciences Research Council (grant no. EP/M015181/1 www.manuGaN.org).The authors gratefully acknowledge Osram for the provision of the GaN/sapphire wafers.

6 References

[1] Meier C., Hennessy K., Haberer E.D., *ET AL.*: 'Visible resonant modes in GaN-based photonic crystal membrane cavities', *Appl. Phys. Lett.*, 2006, **88**, (3), p. 031111
[2] Tchernycheva M., Messanvi A., de Luna Bugallo A., *ET AL.*: 'Integrated photonic platform based on InGaN/GaN nanowire emitters and detectors', *Nano Lett.*, 2014, **14**, (6), pp. 3515–3520
[3] Choi Y.S., Hennessy K., Sharma R., *ET AL.*: 'GaN blue photonic crystal membrane nanocavities', *Appl. Phys. Lett.*, 2005, **87**, (24), p. 243101
[4] Gromovyi M., Semond F., Duboz J.Y., *ET AL.*: 'Low loss GaN waveguides for visible light on Si substrates', *J. Eur. Opt. Soc., Rapid Publ.*, 2014, **9**, p. 14050
[5] Skorka O, Salzman J, Zamir S: 'Coupled waveguides in GaN-based lasers', *J. Opt. Soc. Am. B*, 2003, **20**, (9), pp. 1822–1828
[6] Liu Q., Wang H., He S., *ET AL.*: 'Design of micro-nano grooves incorporated into suspended GaN membrane for active integrated optics', *AIP. Adv.*, 2018, **8**, (11), p. 115118
[7] Chowdhury A., Ng H.M., Bhardwaj M., *ET AL.*: 'Second-harmonic generation in periodically poled GaN', *Appl. Phys. Lett.*, 2003, **83**, (6), pp. 1077–1079

doi: 10.1049/mnl.2019.0366

[8] Ponce F.A., Bour D.P.: 'Nitride-based semiconductors for blue and green light-emitting devices', *Nature*, 1997, **386**, (6623), p. 351
[9] Nakamura S., Fasol G.: 'The blue laser diode: GaN based light emitters and lasers' (Springer Science & Business Media, Germany, 2013)
[10] Shchekin O.B., Epler J.E., Trottier T.A., *ET AL.*: 'High performance thin-film flip-chip InGaN–GaN light-emitting diodes', *Appl. Phys. Lett.*, 2006, **89**, (7), p. 071109
[11] Teisseyre H., Bockowski M., Grzegory I., *ET AL.*: 'GaN doped with beryllium—an effective light converter for white light emitting diodes', *Appl. Phys. Lett.*, 2013, **103**, (1), p. 011107
[12] David A., Fujii T., Moran B., *ET AL.*: 'Photonic crystal laser lift-off GaN light-emitting diodes', *Appl. Phys. Lett.*, 2006, **88**, (13), p. 133514
[13] Zhang C., ElAfandy R., Han J.: 'Distributed Bragg Reflectors for GaN-based Vertical-Cavity Surface-Emitting Lasers', *Appl. Sci.*, 2019, **9**, (8), p. 1593
[14] Wang Y., Chen J., Shi Z., *ET AL.*: 'Suspended membrane GaN gratings for refractive index sensing', *Appl. Phys. Express*, 2014, **7**, (5), p. 052201
[15] Skorka O., Meyler B., Salzman J.: 'Propagation loss in GaN-based ridge waveguides', *Appl. Phys. Lett.*, 2004, **84**, (19), pp. 3801–3803
[16] Chen H., Fu H., Huang X., *ET AL.*: 'Low loss GaN waveguides at the visible spectral wavelengths for integrated photonics applications', *Opt. Express*, 2017, **25**, (25), pp. 31758–31773
[17] Liu Q., Shi Z., Zhu G., *ET AL.*: 'Freestanding GaN grating couplers at visible wavelengths', *J. Opt.*, 2015, **17**, (4), p. 045607
[18] Sekiya T., Sasaki T., Hane K.: 'Design, fabrication, and optical characteristics of freestanding GaN waveguides on silicon substrate', *J. Vac. Sci. Technol. B Nanotechnol. Microelectron., Mater. Process. Meas. Phenom.*, 2015, **33**, (3), p. 031207
[19] Vico Triviño N., Dharanipathy U., Carlin J.F., *ET AL.*: 'Integrated photonics on silicon with wide bandgap GaN semiconductor', *Appl. Phys. Lett.*, 2013, **102**, (8), p. 081120
[20] Hueting N.A., Cryan M.J.: 'Doubly resonant photonic crystal cavities in gallium nitride for fluorescence sensing', *J. Opt. Soc. Am. B*, 2014, **31**, (12), pp. 3008–3017
[21] Vico Triviño N., Minkov M., Urbinati G., *ET AL.*: 'Gallium nitride L3 photonic crystal cavities with an average quality factor of 16,900 in the near infrared', *Appl. Phys. Lett.*, 2014, **105**, (23), p. 231119
[22] Taillaert D., Van Laere F., Ayre M., *ET AL.*: 'Grating couplers for coupling between optical fibers and nanophotonic waveguides', *Jpn. J. Appl. Phys.*, 2006, **45**, (8R), p. 6071
[23] Chausse P.J., Le Boulbar E.D., Lis S.D., *ET AL.*: 'Understanding resolution limit of displacement Talbot lithography', *Opt. Express*, 2019, **27**, (5), pp. 5918–5930
[24] Le Boulbar E.D., Chausse P.J., Lis S., *ET AL.*: 'Displacement Talbot lithography: an alternative technique to fabricate nanostructured metamaterials'. Nanotechnology VIII, Barcelona, Spain, 8 June 2017, vol. 10248, p. 102480Q
[25] Jia S., Le Boulbar E.D., Balram K., *ET AL.*: 'GaN distributed Bragg reflector cavity for sensing applications'. Frontiers in Optics, Washington, DC, USA, 16 September 2018, p. JTu3A-86
[26] Lumerical-Solutions-Inc. Lumerical FDTD Solutions, 2014
[27] Barker A.S.Jr., Ilegems M.: 'Infrared lattice vibrations and free-electron dispersion in GaN', *Phys. Rev. B*, 1973, **7**, (2), p. 743
[28] Malitson I.H.: 'Refraction and dispersion of synthetic sapphire', *J. Opt. Soc. Am.*, 1962, **52**, (12), pp. 1377–1379
[29] Zhang Y., McKnight L., Engin E., *ET AL.*: 'GaN directional couplers for integrated quantum photonics', *Appl. Phys. Lett.*, 2011, **99**, (16), p. 161119
[30] Shields P., Hugues M., Zúñiga-Pérez J., *ET AL.*: 'Fabrication and properties of etched GaN nanorods', *Phys. Status Solidi C*, 2012, **9**, (3–4), pp. 631–634
[31] Dai D., Tang Y., Bowers J.E.: 'Mode conversion in tapered submicron silicon ridge optical waveguides', *Opt. Express*, 2012, **20**, (12), pp. 13425–13439